Utility of a fretting device working under free displacement

G.R. Yantio Njankeu Sabeya, J.-Y. Paris *, J. Denape

Laboratoire de Génie de Production, Ecole Nationale d'Ingénieurs de Tarbes, 47 Avenue d'Azereix, BP 1629, 65016 Tarbes, France

Keywords:
Free displacement conditions in fretting
Seizure
Work of adhesion
Energetic wear coefficient
Titanium alloy
Coating

A B S T R A C T

Relative movements of low amplitudes between two materials in contact are generally reproduced on fretting devices with imposed displacement or imposed tangential force. The damage kinetics observed (cracking, wear) is established under such conditions. In this article, a fretting device working under free displacement is used to characterize the damages generated by seizure and wear. The conditions of seizure are analyzed from the total sliding distance and the discussion is focused on a correlation established with Dupre's work of adhesion. The wear behavior of materials has been characterized from an energetic wear coefficient taking into account the wear volume of contact, the total sliding distance and the dissipated energy.

1. Introduction

Many mechanical assemblies are subjected to vibratory loading stress, resulting from very low amplitude displacements between parts in contact. The micro-sliding generated between surfaces causes well-known damages: cracking and rupture, corrosion or structure transformations, wear with debris formation and seizure [1–5]. These damages are usually studied by imposing either tangential force, or displacement.

- When *tangential force is imposed* (Fig. 1a), the contact adapts by responding in terms of displacement. However, a force controlled test is stable only if it works under partial slip conditions. In full slip conditions, the tangential stiffness is zero when tangential force is proportional to normal force. In this configuration, only cracking is usually studied.
- When *displacement is imposed* (Fig. 1b), the contact adaptation responds in terms of tangential force. In this situation, cracking (nucleation and propagation) and wear (kinetic$\cdots$) depend on displacement amplitude, oscillation frequency and normal load.

In these two approaches, cracking is studied using efficient fatigue criteria [6,7], whereas wear is studied using the "dissipated energy" [8] and "third body" [9] concepts. However, in certain industrial applications, for example blade and disk contact in aircraft turbine engines, recent studies have shown that vibratory instabilities involve great variability in the displacement amplitude [10]. In addition, the authors highlight the free variation of displacement amplitudes during the three flying conditions (take off, hovering and landing). By controlling variable periods of amplitude, a machine working under imposed displacement can generate the free evolution of the displacement.

This article analyzes the damage induced by a contact, which adapts in terms of both tangential force and displacement (Fig. 2). Initially, we describe the function of an experimental device, developed in order to apprehend the complex industrial fretting conditions where effort and displacement amplitudes generally follow uncontrolled variations. Then, we propose to perform a mechanical analysis of this device. In previous articles, we showed that this machine can display seizure conditions [5] and allows the determination of the boundary between seizure and sliding conditions [11]. Seizure is usually defined as the arrest of the relative motion as a result of the adhesive interactions of the rubbing surfaces as well as the debris trapped [12]. In this study, we show that this phenomenon can be carried out by the thermodynamic theory of adhesion [13]. Then, we propose to compare the evolution of wear parameters, such as energetic wear coefficient [11], with thermodynamical parameters, such as work of adhesion. Finally, a physical meaning is proposed for this energetic wear coefficient.

2. Fretting device

2.1. Description

The fretting device used to simulate the fretting phenomena occurring on quasi-static assemblies allows the free evolution of the displacement amplitude (Fig. 3). This machine presents a hemispherical pin-on-disc configuration. Its load capacity ranges

* Corresponding author. Tel.: +33 562 44 27 24; fax: +33 562 44 27 08.
E-mail address: Paris@enit.fr (J.-Y. Paris).

doi:10.1016/j.triboint.2009.04.032

Nomenclature

Device and fretting parameters

P	normal force (N)
P_c	critical normal force (N)
Q	tangential force (N)
δ	real displacement amplitude (μm)
δ_r	referred displacement (μm)
δ_m	measured displacement (m)
δ_o	aperture of the fretting cycle (μm)
δ_{oi}	aperture of the ith fretting cycle (μm)
δ_1, δ_2	deformation due to the bending, respectively, of pin holder and slider (m)
δ_3	relative displacements of the whole assembly surfaces (m)
L	length of the pin holder or of the pin (m)
l	pin radius (m)
S	cross section of the pin holder (m^2)
I	moment of inertia (m^4)
C	measured compliance ($\mu m\,N^{-1}$)
K	stiffness ($N\,\mu m^{-1}$)
C_c	contact compliance ($\mu m\,N^{-1}$)
C_t	tangential compliance ($\mu m\,N^{-1}$)

Materials and coatings properties

t	thickness of coatings (μm)
E	Young's modulus (GPa)
H	hardness (GPa)
Ra	average roughness parameter (μm)
γ	surface free energy ($J\,m^{-2}$)
γ^{LW}	dispersive component of the surface free energy ($J\,m^{-2}$)
γ^{AB}	Lewis acid–base component of the surface free energy ($J\,m^{-2}$)
γ_{12}	interfacial surface free energy ($J\,m^{-2}$)
W_{12}	Dupre's work of adhesion between two substrates in contact ($J\,m^{-2}$)
W_{12}^{LW}	Dupre's work of adhesion due to dispersive Van der Waals interactions ($J\,m^{-2}$)
W_{12}^{AB}	Dupre's work of adhesion due to Lewis acid–base interactions ($J\,m^{-2}$)

Analysis of slip, seizure and damage

D_o	total sliding distance (m)
E_d	dissipated energy (J)
E_{di}	dissipated energy of ith fretting cycle (J)
E_{dt}	total dissipated energy (J)
r	radius of a fretting scar on the slider (m)
R	radius of hemispherical slider (m)
V_c	global wear volume of contact (m^3)
V_d	wear volume of disc (m^3)
V_p	wear volume of slider (m^3)
V^+	wear volume of transfer of matter (m^3)
V^-	wear volume of removal of matter (m^3)
U_c	wear rate of contact ($m^3\,N^{-1}\,m^{-1}$)
GY	energetic wear coefficient ($m^2\,J^{-1}$)

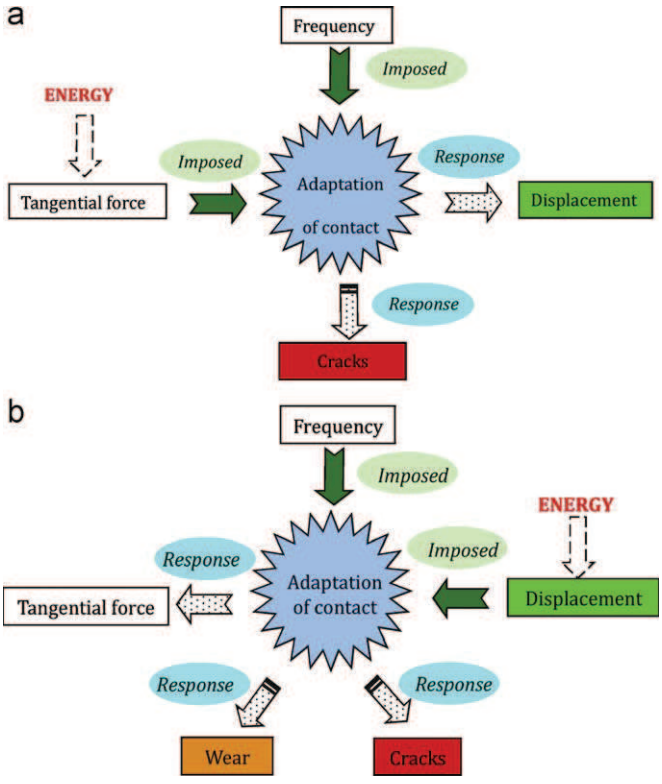

Fig. 1. Approach used for the damage analysis in fretting with a device which: (a) imposed tangential force and (b) imposed displacement.

from 2 to 30 N with initial displacement amplitude ranging from ±10 to ±600 μm and oscillation frequencies of up to 160 Hz.

The rigidity of the device frame is sufficient to prevent the creation of parasitic vibrations of the samples during the test. These dimensions are about 40 cm × 150 cm × 80 cm. The frame supports a platform (reference) provided with four units: an actuator unit, a moving unit, a positioning unit and a loading unit (Fig. 3a).

- The *actuator unit* ① constitutes the vibration generator (exciter). This exciter works on the principle of an electro-magnet that generates alternative movements where displacement and frequency are controlled. The maximum tangential force delivered by the exciter reaches approximately 100 N.

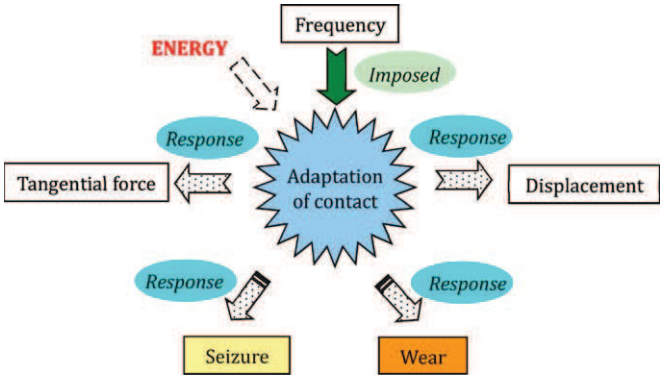

Fig. 2. Approach for the damage analysis in fretting with a device working under free displacement.

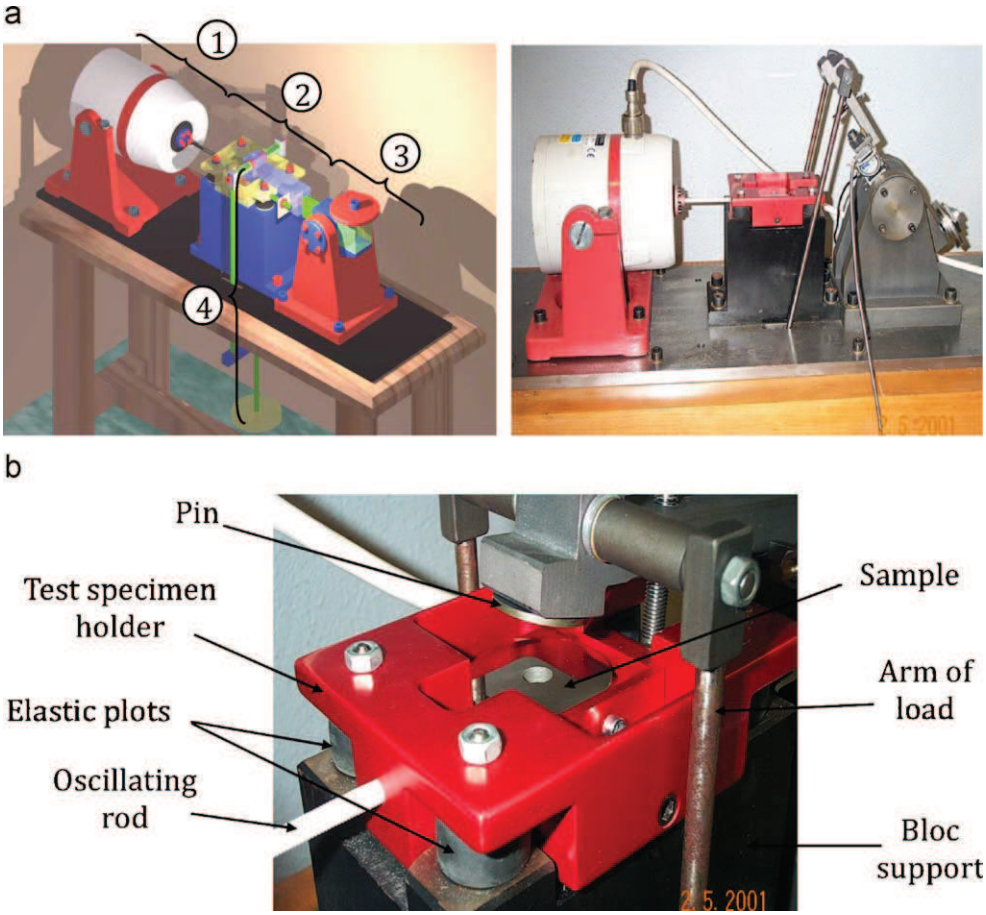

Fig. 3. Fretting device: (a) global view and (b) contact view.

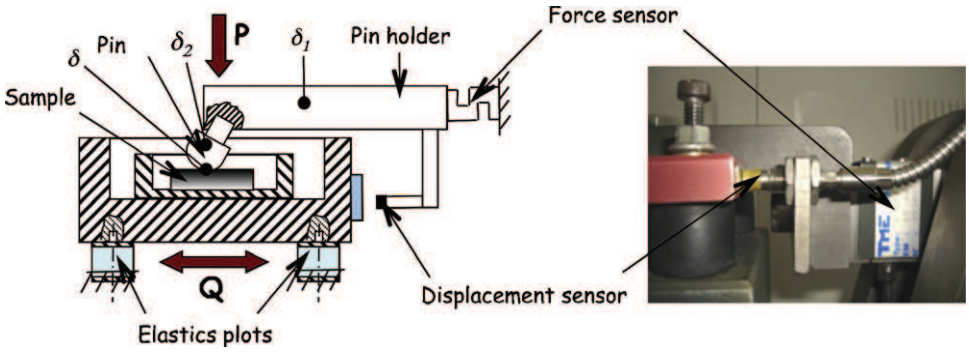

Fig. 4. Position of the force and displacement sensors: (a) schematic representation and (b) real view.

- The *moving unit* (2) is composed of the test specimen holder, four elastic plots (supports) and an oscillating rod (Fig. 3b). The sample holder ensures a horizontal plane of friction. Its shape is designed to fit the friction plane with the leading tangential force. Subjected to significant accelerations, this holder is made of aluminum alloy. The deformation of elastic rubber plots, located at the four corners of the specimen holder ensures the reciprocating motion imposed by the exciter. The oscillating rod transmits the power between the exciter and the sample holder. It also ensures misalignment correction between the sample holder and the exciter.
- The *positioning unit* (3) ensures contact with the pin (slider) and easy removal of the sample between two tests. A counterweight is used to balance the system.
- The *load unit* (4) allows the application of normal force P by using dead weights in line with the contact zone.

A *force sensor* (capacity 100 N), located on the pin holder in the continuity of the friction plan, records the tangential force Q (Fig. 4). The pin holder also carries a contactless *displacement sensor* (inductive sensor) to measure the relative displacement between the slider and the sample.

2.2. Features of fretting device

2.2.1. Real contact displacement

The deformation of the force sensor does not influence the displacement measurement because of its position behind the

displacement sensor. However, deformation due to the bending of pin holder δ_1 and slider δ_2 as well as relative displacements of the whole assembly surfaces δ_3 may involve a contribution to the measured displacement δ_m. The real relative displacement δ between the two contacting bodies can be expressed as

$$\delta = \delta_m - (\delta_1 + \delta_2 + \delta_3) \tag{1}$$

The contribution to δ_3 is negligible because surfaces are maintained tight by screwing. Moreover, the displacements δ_1 and δ_2 can be calculated as

$$\delta_1 = \frac{Q\,L}{E\,S} \quad \text{and} \quad \delta_2 = \frac{Q\,L^3}{3\,E\,I} \quad \text{with } I = \frac{\pi\,l^4}{4} \tag{2}$$

where Q is the tangential force, L and S are the length and the cross section of the pin holder, respectively, E is the material Young's modulus, I is the moment of inertia and l is the pin radius.

For a tangential force of 15 N, the deformation calculus of the steel pin holder ($E = 210$ GPa, length $L = 115$ mm, $S = 0.522$ m^2) gives $\delta_1 = 1.6 \times 10^{-2}$ μm. The deformation of the titanium alloy slider ($E = 122$ GPa, $L = 10$ mm, $l = 5$ mm) reaches only $\delta_2 = 0.00009$ μm. These displacements are negligible. Consequently, the displacement measured corresponds to the real displacement of the contact, i.e.

$$\delta_m = \delta \tag{3}$$

2.2.2. Specificity of the fretting device

The device is driven in open-loop control mode, i.e. the system does not impose displacement amplitude, as is the case with most traditional fretting devices. Consequently, the real displacement is directly linked to the friction forces generated in the contact. After adjustment at a referred displacement δ_r, the sliding materials are put into contact. Because of friction occurrence, measurement of the real displacement δ is systematically lower than referred displacement δ_r. The amplitude of real displacement δ evolves freely throughout the test (Fig. 5a). A direct relation between δ and tangential force Q is observed (Fig. 5b): an increase in tangential force generates a reduction in displacement amplitude. Consequently, this device can lead to seizure [5].

2.2.3. Compliance of the contact

The effect of fretting device compliance is studied through hysteresis loops. Several authors have proved that compliance influences the measured displacement [14–16]. It depends on material composition as well as on system configuration (device). Thus, the relative displacement measured by the inductive sensor is the sum of the tangential displacements resulting from elastic deformation of the various mechanical parts included in the measuring equipment.

The measured compliance C, inverse of the tangential stiffness K, is the sum of the contact compliance C_c and the tangential compliance C_t. We can write

$$C_t = C - C_c \tag{4}$$

Moreover, according to Fouvry et al. [15], the expression of the contact displacement δ can expressed by

$$\delta = \delta_m - C_t \cdot Q \tag{5}$$

As the displacement sensor measures the real displacement directly, the tangential compliance is nil. Thus, measured compliance C proves to be the contact compliance. This compliance does not remain constant and evolves freely during the test (Fig. 6).

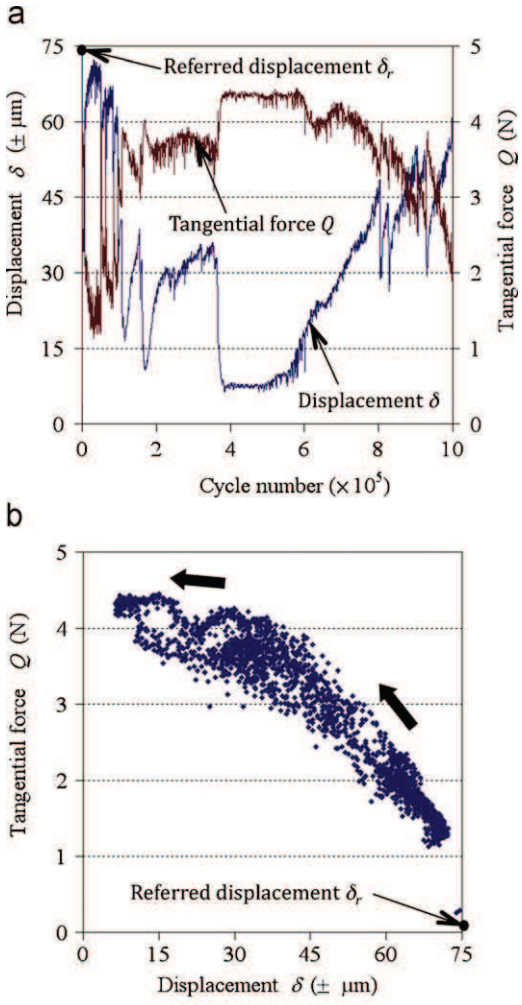

Fig. 5. (a) Displacement amplitude δ and tangential force Q as a function of the number of cycles and (b) relationship between tangential force Q and displacement amplitude δ. Case of nitriding+DLC ($\delta_r = \pm 75$ μm, $P = 6$ N).

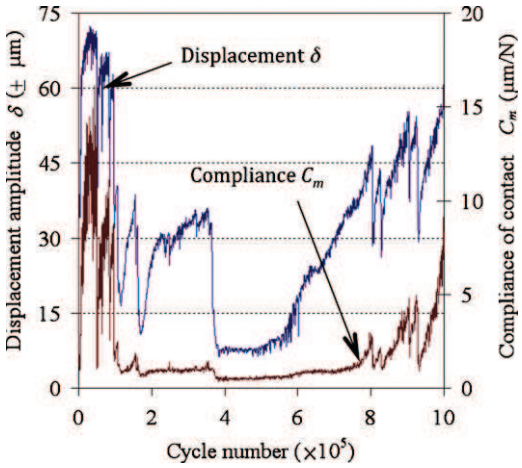

Fig. 6. Displacement amplitude δ and measured compliance of the contact C_m as a function of the number of cycles. Case of nitriding+DLC ($\delta_r = \pm 75$ μm, $P = 6$ N).

2.3. Materials studied and experimental conditions

Samples and pins are made of Ti–6Al–4V, an α+β titanium alloy. Because of their highly specific properties, these materials

are usually used in the aircraft industry to reduce structure weight while preserving high mechanical characteristics. Some Ti–6Al–4V samples were subjected to a nitriding treatment carried out at 600 °C for 12 h using plasma obtained from a gas mixture of 80% N_2+20% H_2. The nitrided layers (ε-Ti_2N) are approximately 0.25 μm thick, with a diffusion profile of nitrogen (diffusion layer of α-TiN) about 1 μm deep. Some treated disks were also coated with an amorphous diamond-like carbon DLC layer, 1 μm thick. This layer was deposited by PACVD (plasma assisted chemical vapor deposition) using pure CH_4 as a source gas under the following conditions: pressure 1.33 Pa, tension of self-polarization 150 V, time of deposit 4 h, generator power 150 W.

Untreated samples were coated with a copper–nickel–silicon (CuNiSi) or a copper–nickel–indium (CuNiIn) layer. The CuNiSi coatings were obtained by PVD (magnetron sputtering) and were from 10 to 12 μm thick. The CuNiIn coatings were deposited by plasma spraying. These coatings are 125–150 μm thick. An additional organic layer covers some CuNiIn coatings. This organic coating embeds a solid lubricant (molybdenum disulphide MoS_2) and its thickness ranges from 15 to 20 μm.

The hemispherical pins (radius of curvature 10 mm) are not coated. They received only shot-peening treatment carried out according to the standard AFNOR NFL 06832 (ball diameter of 0.315 mm, ALMEN intensity of 0.15 mm, overlap of 125%). This operation involves a modification of surface roughness and a generation of compressive residual stresses of about 1 GPa through a depth of approximately 100 μm.

The topographic and mechanical properties of Ti–6Al–4V and coatings are given in Table 1. The values of Young modulus E and hardness H were obtained by nano-indentation tests. The thickness t was measured on transverse sections and the roughness parameters Ra were obtained by interferometric profilometry.

The fretting tests were carried out at a constant frequency of 100 Hz and at an ambient temperature over a period corresponding to 10^6 cycles. The normal load ranges from 2.5 to 15 N with referred displacement amplitudes δ_r of ±50, ±75 and ±100 μm.

3. Results and discussions

3.1. Seizure analysis

3.1.1. Description

The arrest of relative motion, resulting from a sudden rise in the tangential force, appears as soon as the contact is set between the two materials. The seizure is simultaneously identified by a strong reduction in displacement amplitude and by the closing of the cycle (Fig. 7a). This seizure regime (SR) can be maintained all along the test. A delayed seizure regime (DSR) can also be observed: a phase of sliding followed by a phase of seizure sometimes occurs (Fig. 7b). In this situation, a drop towards low amplitude affects the displacement.

Table 1
Topographic and mechanical properties of Ti–6Al–4V and coatings.

Materials	t (μm)	Ra (μm)	E (GPa)	H (GPa)
Ti–6Al–4V	–	0.07	122±1	5.4±0.3
Nitriding+DLC	0.25+1	0.8	164±58	16±7
CuNiSi	10–12	0.6	84±3	2.9±0.5
CuNiIn	125–150	11.6	75±7	2.1±0.1
Polymer bonded MoS_2	15–20	5	12±1	0.42±0.01

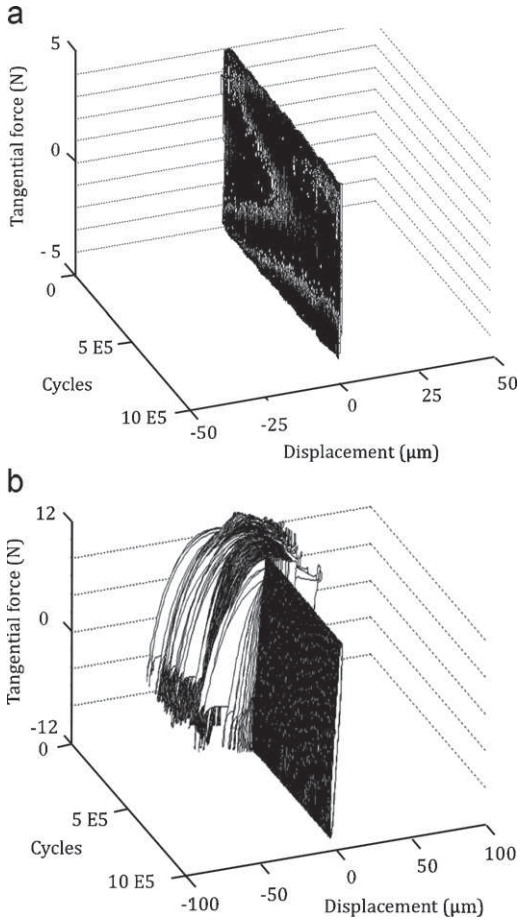

Fig. 7. Contact responses: (a) seizure regime: case of Ti–6Al–4V ($\delta_r = \pm 50$ μm, $P = 10$ N) and (b) delay seizure regime: case of nitriding+DLC ($P = 15$ N, $\delta_r = \pm 100$ μm).

3.1.2. Seizure thresholds

Under free displacements, cycle aperture δ_o evolves during the test with regard to displacement δ (Fig. 8). For a given referred displacement δ_r and a similar cycle number N, the real sliding distance appears very differently from one pair of material to another. The total sliding distance becomes a relevant parameter in providing information on the ability of the material to delay the seizure phenomenon. This distance D_o is defined from the measurements of the overall cycle apertures δ_{oi} before seizure:

$$D_o = 4 \sum_{i=0}^{Seizure} \delta_{oi} \tag{6}$$

The normal load influences the sliding period and thus the seizure conditions. As expected, the total sliding distance D_o decreases with the increase in normal loads for a given referred displacement, δ_r (Fig. 9). It increases along with the rise in referred displacement. The seizure condition is obtained by extrapolating the curve $D_o(P)$ towards a sliding distance equal to zero. The critical normal loads P_c (extrapolated point), corresponding to seizure conditions for the materials studied, are summarized in Table 2. These critical loads were experimentally confirmed as shown in Fig. 10. The cycle apertures observed, at the beginning of the tests at 7 N at ±75 μm and at 8.5 N at ±75 μm, may result from initial friction on contaminant screens before the establishment of the real contact between the solid surfaces.

The critical normal loads logically increase with the rise in referred displacement. Furthermore, Ti–6Al–4V, known for its

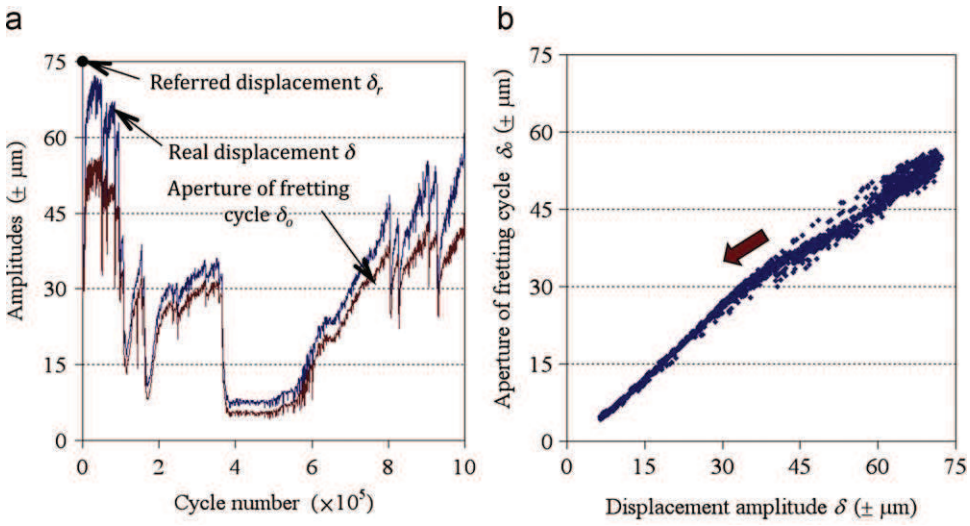

Fig. 8. (a) Displacement amplitude δ and cycle aperture δ_o as a function of the number of cycles and (b) relationship between cycle aperture δ_o and displacement amplitude δ. Case of nitriding+DLC ($\delta_r = \pm 75\,\mu m$, $P = 6\,N$).

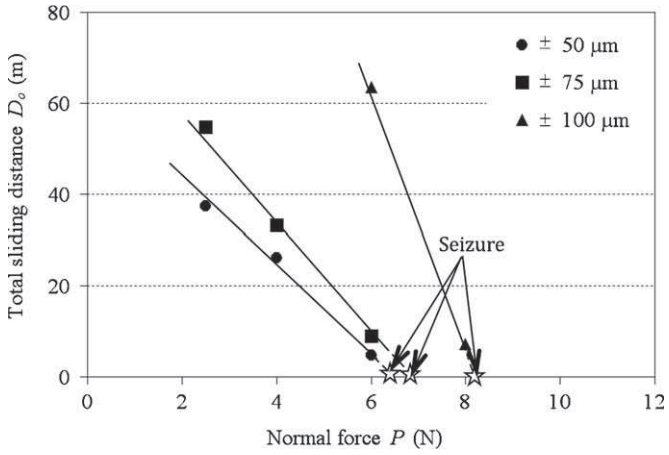

Fig. 9. Evolution of the total sliding distance D_o as a function of the normal force P. Case of Ti–6Al–4V/Ti–6Al–4V contact.

Table 2
Critical normal loads P_c (extrapolated point) corresponding to seizure conditions for Ti–6Al–4V and coatings.

Materials	±50 µm	±75 µm	±100 µm
Ti–6Al–4V	6.6	6.9	8.5
Nitriding+DLC	10	15.4	18.9
CuNiSi	9.5	11.8	15.8
CuNiIn	9	11	15.5
CuNiIn+polymer bonded MoS_2	11.98	20.6	102.2

high seizure sensitivity, presents lower seizure loads compared to other materials. Cupronickels coatings show similar seizure thresholds but they are higher than those of Ti–6Al–4V. Association of nitriding and DLC combination, as cupronickel coatings, seems to be a solution able to delay the seizure phenomena efficiently. However, the highest seizure thresholds are obtained with the CuNiIn and polymer bonded solid lubricant (MoS_2).

3.1.3. Thermodynamic approach to adhesion

An early reduction of the sliding amplitude involves a low total sliding distance. The chemical composition of the material surfaces can thus influences seizure conditions and so seizure can be analyzed using the thermodynamic theory of adhesion [13]. The nature of the bonding interactions on a solid surface can be studied using the wettability method. The surface free energy γ of each material was determined by the sessile-drop technique using a Digidrop goniometer from GBX Instruments. The contact angles were determined using the one-liquid method of the Fowkes procedure [17]. According to Fowkes, we have

$$\gamma = \gamma^{Lw} + \gamma^{AB} \tag{7}$$

where γ^{Lw} represents the component for long distance (>0.4 nm) dispersive Lifschitz–Van der Waals interactions and γ^{AB} is the component related to short distance (<0.4 nm) Lewis acid–base interactions. Table 3 gathers the surface free energies of the studied materials.

Dupre's work of adhesion W_{12} between two solids constitutes a relevant surface parameter to interpret the seizure phenomena:

$$W_{12} = \gamma_1 + \gamma_2 - \gamma_{12} \tag{8}$$

where γ_1, γ_2 and γ_{12} represent the surface free energies of materials (referred as 1 and 2) and the interfacial surface free energy, respectively. This work also depends on additive dispersive Van der Waals and Lewis acid–base interactions [17]:

$$W_{12} = W_{12}^{LW} + W_{12}^{AB} \tag{9}$$

$$W_{12}^{LW} = 2(\gamma_1^{LW}\gamma_2^{LW})^{1/2} \quad \text{and} \quad W_{12}^{AB} = 2(\gamma_1^{AB}\gamma_2^{AB})^{1/2} \tag{10}$$

The relationship $D_o = f(W_{12})$ shows a noticeable result (Fig. 11): the total sliding distance D_o increases when the work of adhesion W_{12} decreases, i.e. when the adhesive interactions decrease. This result means that a material pair will *a priori* be able to delay the seizure phenomena if it reveals low work of adhesion. As expected, the Ti–6Al–4V alloy, well known for its high seizure sensitivity, presents a high work of adhesion and its total sliding distance is quite low. On the other hand, the CuNiIn+polymer coating presents a low work of adhesion and leads to a much greater total sliding distance.

3.2. Wear analysis

3.2.1. Wear quantification

Surface damages are observed in delay seizure and full slip regimes. The surface degradations result from material removal

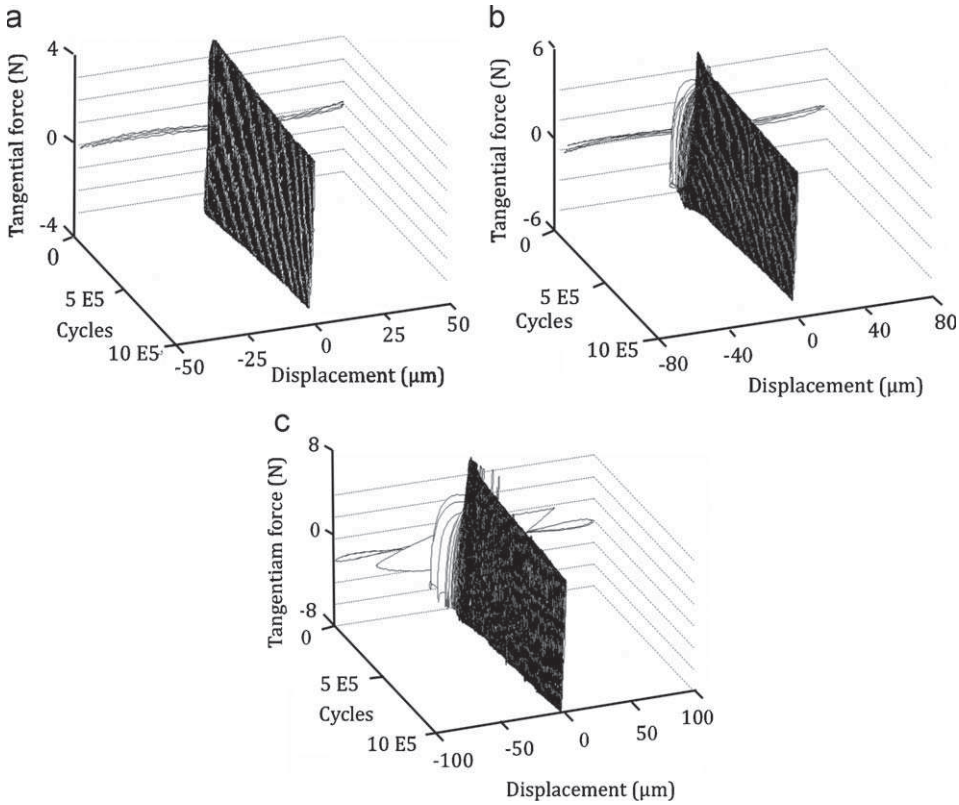

Fig. 10. Friction logs in the seizure regime for the Ti–6Al–4V/Ti–6Al–4V contact: (a) $\delta_r = \pm 50\,\mu m$, $P = 6.4\,N$; (b) $\delta_r = \pm 75\,\mu m$, $P = 7\,N$ and (c) $\delta_r = \pm 100\,\mu m$, $P = 8.5\,N$.

Table 3
Surface free energies, γ, of Ti–6Al–4V and coatings.

Samples	γ^{LW} (mJ m^{-2})	γ^{AB} (mJ m^{-2})	γ (mJ m^{-2})
Ti–6Al–4V	36.4±0.7	12.8±0.4	49.2±2.5
CuNiSi	42.7±0.9	1.7±0.1	44.4±2.2
CuNiIn	42.8±0.9	1.0±0.1	43.8±2.2
Nitriding+DLC	40.6±0.8	3.2±0.1	43.8±2.2
CuNiIn+polymer bonded MoS_2	35.7±0.7	0.2±0.01	35.9±1.8

γ^{Lw} represents the component for long distance dispersive Lifschitz–Van der Waals interactions and γ^{AB} is the component related to short distance Lewis acid–base interactions.

with debris forming inside the fretting scar and debris ejection outside the contact zone (Fig. 12). The wear parameters were calculated from 3D profiles of the fretting scars obtained by optical profilometry. The volumes V_d and V_p of samples and pins, respectively, are defined as

$$V_d = V_d^- - V_d^+ \quad \text{and} \quad V_p = \frac{\pi r^4}{4R} \tag{11}$$

Volume V_d^- corresponds to the lost material situated below the initial surface level while volume V_d^+ is related to transfer material above the initial surface level inside the contact zone (Fig. 13a). Volume V_p is calculated from the measurement of the radius r on the pin scar, related to the approximation $r \ll R$ where R is the hemispheric pin radius (Fig. 13b). The amount of material lost by the contacting bodies, i.e. the wear volume of the contact V_c is given by

$$V_c = V_d + V_p \tag{12}$$

This formula qualifies the contact as a whole, both in terms of sample degradation and of aggressivity over the slider.

3.2.2. Wear rate approach

The wear evaluation methodology of our material pairs is illustrated by the Ti–6Al–4V/Ti–6Al–4V contact. The increase of wear volume with the total sliding distance (Fig. 14) suggests that degradation mechanisms are similar whatever the test conditions. Moreover, the effective wear volume of the contact V_c/D_o for a given referred displacement decreases with the rise in the normal force P (Fig. 15). When the normal force threshold is reached, wear no longer occurs. In addition, for a given normal force, the effective wear volume increases with referred displacement δ_r. Finally, the evolutions of effective wear volume V_c/D_o as a function of normal force P show that this quantity also depends on referred displacement δ_r. Thus, the traditional Archard expression of the wear rate, defined as

$$U_c = \frac{V_c}{PD_o} \tag{13}$$

still depends on referred displacement δ_r which is related directly to energy initially introduced into the contact (Fig. 16). So, a formula based on Archard's theory fails to predict fretting wear when displacement amplitude varies. This result is confirmed by studies on devices working under controlled displacement, when variable amplitudes of gross slip sequences are imposed [10,18]. Consequently, it appears necessary to introduce a more robust and general criterion that is able to quantify the wear behavior of materials by taking into account the tribological parameters of the contact as a whole.

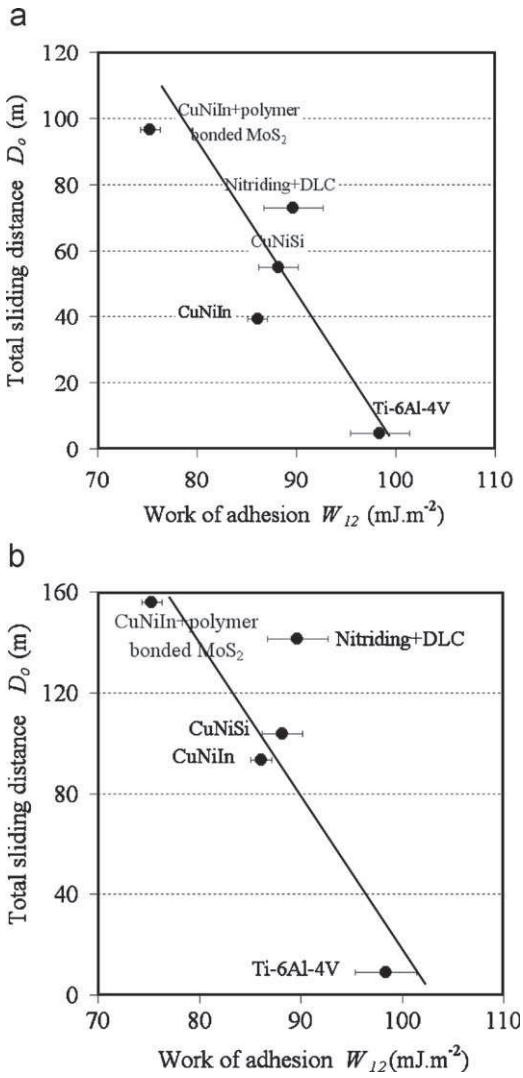

Fig. 11. Relationship between the total sliding distance and the work of adhesion: (a) $\delta_r = \pm 50\,\mu m$, $P = 6\,N$ and (b) $\delta_r = \pm 75\,\mu m$, $P = 6\,N$.

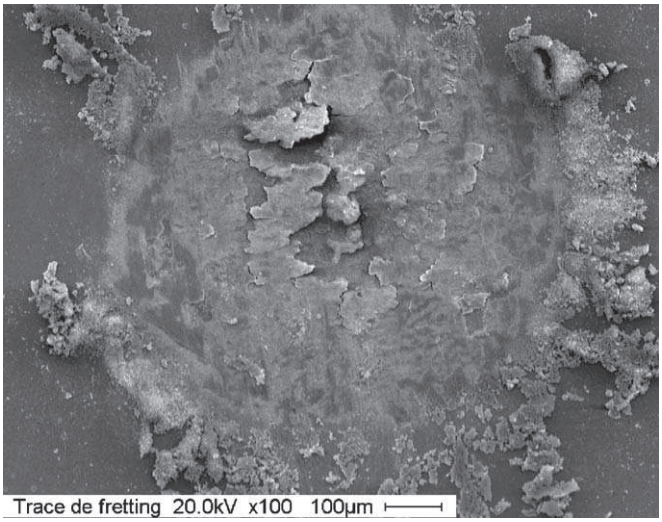

Fig. 12. Fretting scar for Ti–6Al–4V/Ti–6Al–4V contact ($\delta_r = \pm 75\,\mu m$, $P = 4\,N$).

3.2.3. Introduction of an energetic wear coefficient

The product of tangential force and measured displacement represents the dissipated energy E_d in the contact. For each fretting cycle, this energy, E_{di}, pertains to the area of the fretting cycle. The total dissipated energy E_{dt} within the contact is defined as the sum of the fretting cycle areas before seizure. By plotting the effective wear volume V_c/D_o as a function of the total dissipated energy E_{dt} for a given material pair, all values are joined together on a single main curve independently of normal force P and the referred displacement δ_r (Fig. 17). This result justifies the introduction of an energetic wear coefficient GY, which represents the slope of this master curve [11]:

$$GY = \frac{V_c}{D_o \cdot E_{dt}} \tag{14}$$

This energetic wear coefficient is expressed in $m^2\,J^{-1}$ (inverse of a surface energy) whereas wear rate is expressed in $m^3\,N^{-1}\,m^{-1}$ (inverse of a pressure). This energy coefficient takes into account not only the wear volume of the contact but also the total sliding distance and the dissipated energy. The appearance of a dimensionally surface term in this energetic wear coefficient suggests that the amount of surface created is a more relevant parameter than the volume of removed material. That could mean that a given wear volume can produce various sizes of debris characterized by different surface extensions (different specific surface areas; Fig. 18). The more surface formed, the greater the adhesion mechanisms involved. The fretting wear of materials working under free displacement conditions can be characterized judiciously by the energetic wear coefficient GY while a volumetric energy coefficient seems more relevant to fretting wear in relation to imposed displacement conditions. A good wear behavior corresponds to a low energetic coefficient of wear GY. The various energetic wear coefficients of materials show that the cupronickels alloys CuNiIn and CuNiSi coatings register energetic wear coefficients similar to those of Ti–6Al–4V (Table 4). This energetic wear coefficient is significantly reduced with nitriding+DLC and CuNiIn+polymer bonded lubricant coatings.

3.2.4. Relationship between wear parameter and work of adhesion

Mechanisms of matter removal or matter transfer induce adhesion phenomena in the contact. Energy required to surface generation can be linked to the work of adhesion W_{12}. In addition, the wear behavior of materials illustrates their ability to create new surfaces, as expected by the energetic wear coefficient GY.

Fig. 19 reveals the relationship between energetic wear coefficient GY, and work of adhesion W_{12}, and shows two distinct trends depending on the composition of the contacting pairs. For cupronickel coatings, the energetic wear coefficient increases with the work of adhesion, i.e. adhesive interactions accelerate the wear process of cupronickel coatings. However, the energetic wear coefficient of nitriding+DLC coating is similar to that of CuNiIn+MoS_2 coating, whereas its work of adhesion is larger. It appears that mechanisms for creating, trapping and ejection of debris also play a significant influence on wear behavior of materials.

4. Conclusion

The wear and seizure behavior of various coating materials against a titanium alloy were studied under fretting conditions where the contact adapts by giving a response in terms of both tangential force and displacement.

The seizure ability was quantified by extrapolating the critical normal force corresponding to a total sliding distance equal to 0. Untreated Ti–6Al–4V alloy, already known for its high seizure sensitivity, logically presents a lower seizure threshold in terms of critical normal force than the other materials. This seizure threshold is enhanced by the presence of CuNiSi, CuNiIn and

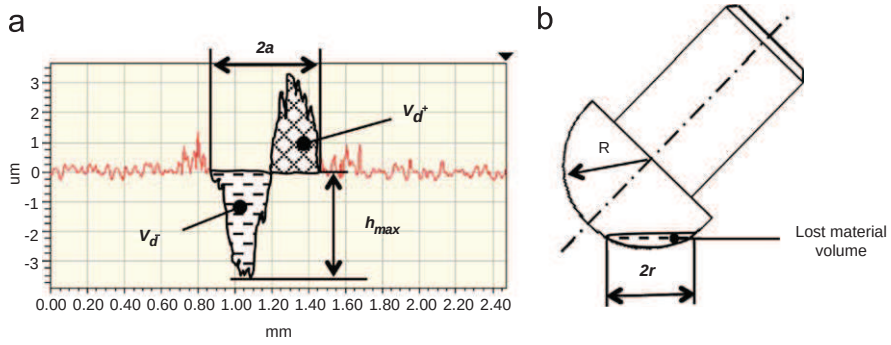

Fig. 13. (a) Profile of wear scar extracted on the disk, with removal and transfer of matter and (b) example of fretting scar on the pin.

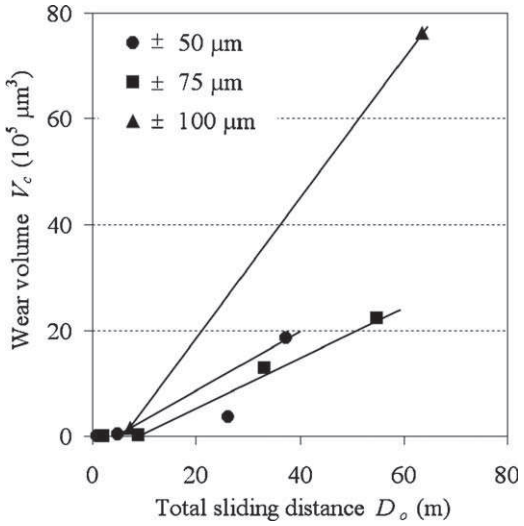

Fig. 14. Evolution of wear volume of contact as a function of the total sliding distance for the Ti–6Al–4V/Ti–6Al–4V contact.

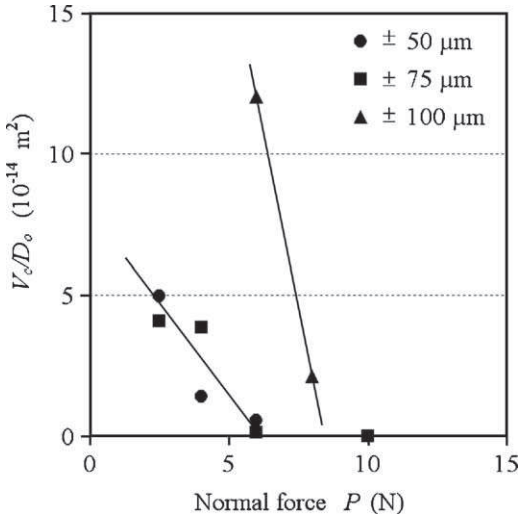

Fig. 15. Evolution of effective wear volume V_c/D_o as a function of the normal force P for the Ti–6Al–4V/Ti–6Al–4V contact.

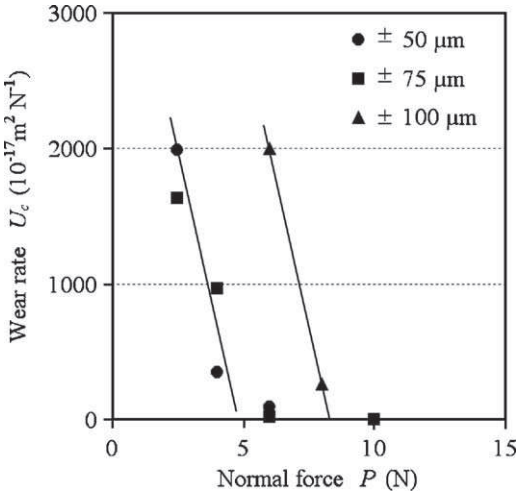

Fig. 16. Evolution of wear rate U_c as a function of the normal load P for the Ti–6Al–4V/Ti–6Al–4V contact.

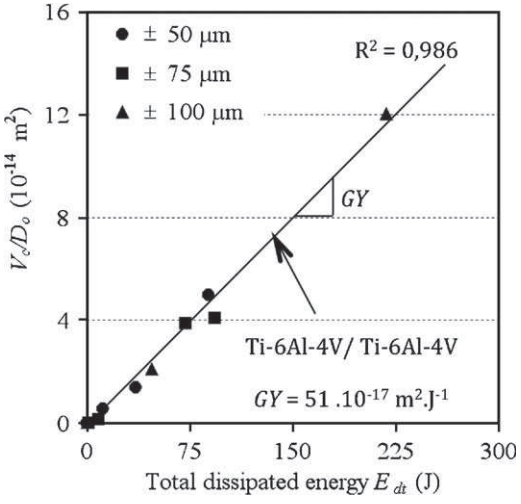

Fig. 17. Evolution of effective wear volume V_c/D_o as a function of the normal load P for the Ti–6Al–4V/Ti–6Al–4V contact.

nitriding+DLC coatings. The CuNiIn+polymer bonded solid lubricant MoS_2 still strongly increases this seizure threshold and gives the best performance. These results are in high correlation with the total sliding distance and Dupre's work of adhesion. Thus, the CuNiIn+polymer presented a low work of adhesion for high sliding distances whereas Ti–6Al–4V presented a higher work of adhesion for a low sliding distance.

The wear analysis shows that the wear volumes cannot be compared directly because the total sliding distance D_o differs for every material despite a same number of cycles (as a consequence of the experimental device working under free displacement). Wear rate results also show that the effective wear volume still

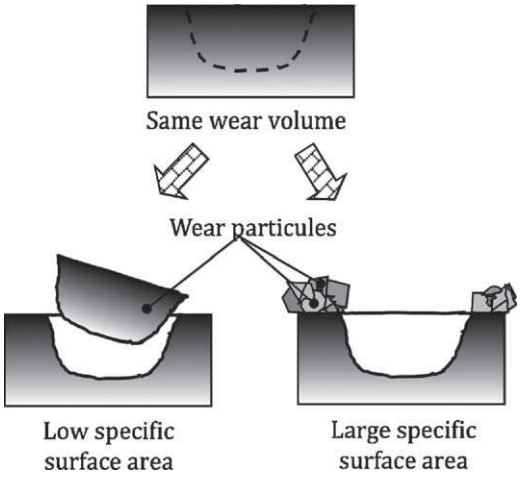

Fig. 18. Illustration of wear of a material.

Table 4
Wear energetic coefficient of Ti–6Al–4V and coatings.

Ti–6Al–4V	CuNiIn	CuNiSi	Nitriding+DLC	CuNiIn+polymer bonded MoS_2
51 ± 7	67 ± 9	47 ± 6	11 ± 1	8 ± 1

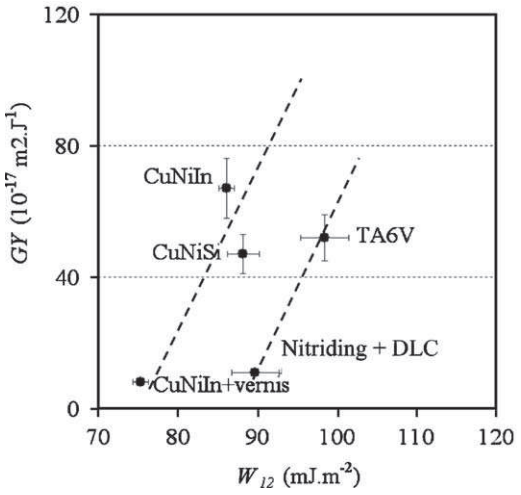

Fig. 19. Relationship between wear and work of adhesion for the couple of materials studied.

depends on the referred displacement, i.e. on the initial energy introduced into the contact. An energetic wear coefficient, taking into consideration the wear volume of the contact, the total sliding distance and the total dissipated energy, allows the comparison of all materials for different test conditions. Thus, the nitriding+DLC and CuNiIn+polymer coatings have a low energetic coefficient of wear compared to Ti–6Al–4V, CuNiIn and CuNiSi coatings, which register comparable energy coefficients of wear. Although the work of adhesion is determined on surfaces not affected by friction, we find a satisfactory correlation between this thermodynamic parameter and the energetic wear coefficient. However, it appears that mechanisms for creating, trapping and ejection of debris also play a significant influence on wear behavior of materials.

Acknowledgements

This study was supported by Snecma Moteurs (France) and the Education and Research Minister (France). The authors thank MM. Jean-Michel de Monicault, Thomas Ganne from Snecma Moteurs, MM. Luc Pichon and Jean-Paul Rivière from Laboratoire de Métallurgie Physique of Poitiers (France) for providing the samples and for helpful discussions.

References

[1] Waterhouse RB, Taylor DE. Fretting debris and delamination theory of wear. Wear 1974;29:337–44.
[2] Lindley TC, Nix KJ. The role of fretting in the initiation and early growth of fatigue cracks in turbo-generator materials. ASTM STP 1982;85:340.
[3] Sauger E, Fouvry S, Ponsonnet L, Kapsa P, Martin J, Vincent L. Tribologically transformed structure in fretting. Wear 2000;245:39–52.
[4] Vincent L. Materials and fretting. ESIS 18. Mechanical Engineering Publication; 1994. p. 323–37.
[5] Yantio Njankeu GR, Paris J-Y, Denape J, Pichon L, Riviere J-P. Study of seizure of coated and treated titanium alloy under fretting conditions. Tribology International 2006;39:1052–9.
[6] Proudhon H, Fouvry S, Yantio GR. Determination and prediction of the fretting crack initiation: introduction of the (*P, Q, N*) representation and determination of a variable process volume. International Journal of Fatigue 2006;28:707–13.
[7] Fouvry S, Elleuch K, Simeon G. Prediction of crack nucleation under partial slip fretting conditions. Journal of Strain Analysis 2002;37(6):549–64.
[8] Mohrbacher H, Blanpain B, Celis JP, Roos JR, Stals L, Van Stappen M. Oxidational wear of TiN coating on tool steel and nitrided tool steel in unlubricated fretting. Wear 1995;188:130–7.
[9] Godet M. The third body approach, a mechanical view of wear. Wear 1984;100:437–52.
[10] Paulin C, Fouvry S, Deyber S. Wear kinetics of Ti–6Al–4V under constant and variable (gross slip) fretting sliding conditions. Wear 2005;259(1–6):292–9.
[11] Yantio Njankeu Sabeya GR, Paris J-Y, Denape J. Fretting wear of a coated titanium alloy under free displacement. Wear 2008;264:166–76.
[12] Williams JA. Engineering tribology. Oxford University Press; 1994.
[13] Lambert M, Duluc S, Paris J-Y, Baziard Y, Denape J. Work of adhesion and fretting: influence of material surface properties and medium. Surface and Interface Analysis 2002;34:790–3.
[14] Vingsbo OB. Fretting and contact fatigue studied with the aid of fretting maps. ASTM STP 1992;1159:49.
[15] Fouvry S, Kapsa Ph, Vincent L. Quantification of fretting damage. Wear 1996;200:186–205.
[16] Ramalho A, Celis J-P. Fretting laboratory tests: analysis of mechanical response of test rigs. Tribology Letters 2003;14(3):187–96.
[17] Fowkes FM. Rubber Chemistry and Technology 1984;57:328.
[18] Fouvry S, Paulin C, Deyber S. Impact of contact size and complex gross-partial slip conditions on Ti–6Al–4V/Ti–6Al–4V fretting wear. Tribology International 2009;42:461–74.